Biochemical and Biophysical Research Communications 450 (2014) 634–640

Contents lists available at ScienceDirect

Biochemical and Biophysical Research Communications

journal homepage: www.elsevier.com/locate/ybbrc

Structural analysis of the yeast exosome Rrp6p–Rrp47p complex by small-angle X-ray scattering

Emil Dedic [a,c], Paulina Seweryn [a,c], Anette Thyssen Jonstrup [a,c], Rasmus Koch Flygaard [a,c], Natalya U. Fedosova [d], Søren Vrønning Hoffmann [e], Thomas Boesen [b,c], Ditlev Egeskov Brodersen [a,c,*]

[a] Centre for mRNP Biogenesis and Metabolism, Gustav Wieds Vej 10c, Aarhus University, DK-8000 Aarhus C, Denmark
[b] Centre for Membrane Pumps in Cells and Disease – PUMPKIN, Gustav Wieds Vej 10c, Aarhus University, DK-8000 Aarhus C, Denmark
[c] Department of Molecular Biology and Genetics, Gustav Wieds Vej 10c, Aarhus University, DK-8000 Aarhus C, Denmark
[d] Department of Biomedicine, Ole Worms Allé 6, Aarhus University, DK-8000 Aarhus C, Denmark
[e] Institute for Storage Ring Facilities (ISA), Department of Physics and Astronomy, Ny Munkegade 120, Aarhus University, DK-8000 Aarhus C, Denmark

ARTICLE INFO

Article history:
Received 29 May 2014
Available online 14 June 2014

Keywords:
Exosome
3′–5′ nuclease
RNA turnover
RNA processing
snoRNA
Ribosomal RNA

ABSTRACT

The RNase D-type 3′–5′ exonuclease Rrp6p from *Saccharomyces cerevisiae* is a nuclear-specific cofactor of the RNA exosome and associates *in vivo* with Rrp47p (Lrp1p). Here, we show using biochemistry and small-angle X-ray scattering (SAXS) that Rrp6p and Rrp47p associate into a stable, heterodimeric complex with an elongated shape consistent with binding of Rrp47p to the nuclease domain and opposite of the HRDC domain of Rrp6p. Rrp47p reduces the exonucleolytic activity of Rrp6p on both single-stranded and structured RNA substrates without significantly altering the affinity towards RNA or the ability of Rrp6p to degrade RNA secondary structure.

1. Introduction

The eukaryotic RNA exosome is involved in a multitude of processes including maturation of stable RNAs, turnover of messenger RNA as well as scavenging of aberrant, poly-adenylated nuclear transcripts and short transcripts arising from pervasive transcription [1,2]. Structurally, the exosome consists of a ring of six proteins homologous to bacterial RNase PH and three RNA-binding "cap" proteins, known as the "exosome core" [3,4]. In *Saccharomyces cerevisiae*, the exosome ring has lost catalytic activity and ubiquitously associates with Rrp44p/Dis3p, which functions as both 3′–5′ exonuclease and as endonuclease [5,6]. In the yeast nucleus, the complex additionally binds the RNase D-type 3′–5′ exonuclease, Rrp6p, which is required for stable RNA processing and turnover specific to this compartment [7–9]. Crystal structures currently exist of the human exosome core as well as the core bound to Rrp44p and a C-terminal peptide from Rrp6p showing that Rrp6p binds at the "top" of the core, opposite Rrp44p [3,10]. In addition, crystal structures exist of the isolated exonuclease core domains of yeast, Trypanosoma, and human Rrp6p [11–13].

Rrp6p consists of an N-terminal PMC2NT region and a DEDD-type 3′–5′ exonuclease domain homologous to bacterial RNase D and at least one Helicase and RNase D C-terminal (HRDC) domain [9]. The available crystal structures of Rrp6p all encompass a part of the N-terminus unique to eukaryotes, the exonuclease core, and one HRDC domain [11–13]. These structures have revealed a compact nuclease domain with the N-terminus wrapped around it and a more loosely associated HRDC domain, homologous to the first of two HRDC domains found in *Escherichia coli* RNase D [14]. *In vitro*, isolated Rrp6p is active as a 3′–5′ exonuclease on a range of both single-stranded and structured RNA substrates with a subtle preference for poly-A RNA [3,7,12]. via its N-terminal PMC2NT region, Rrp6p interacts with an additional exosome cofactor, Rrp47p (Lrp1p), which exists as a multimer in isolation, but appears to associate with Rrp6p in a 1:1 complex [11,15]. Furthermore, yeast Rrp47p has been shown to specifically bind double-stranded nucleic acids *in vitro* but sequence analysis has so far failed to identify any known RNA binding domains [16,17]. Rrp47p

Abbreviations: SAXS, small-angle X-ray scattering; HRDC, helicase and RNase D C-terminal domain; snoRNP, small nucleolar ribonucleoprotein; SRCD, synchrotron radiation circular dichroism; RALS, right-angle light scattering; MALS, multi-angle light scattering; FAM, 5′ carboxy-fluorescein; SEC, size-exclusion chromatography; EMSA, electrophoretic mobility shift assay; MW, molecular weight.

* Corresponding author at: Department of Molecular Biology and Genetics, Gustav Wieds Vej 10c, Aarhus University, DK-8000 Aarhus C, Denmark. Fax: +45 8612 3178.
E-mail address: deb@mb.au.dk (D.E. Brodersen).

http://dx.doi.org/10.1016/j.bbrc.2014.06.032
0006-291X/

is present in pull-down experiments targeting core exosome subunits indicating that it forms a natural part of at least a population of nuclear exosomes, but the details of the interplay between the exosome core, Rrp6p, and Rrp47p are not yet understood [18].

Deletion of either Rrp6p or Rrp47p results in accumulation of 3′ extended forms of both 5.8S ribosomal RNA and snoRNAs in yeast [18,19]. Moreover, the PMC2NT region of Rrp6p is required for correct RNA processing as well as for normal levels of Rrp47p strongly supporting that the two proteins are naturally bound to each other *in vivo* [15,17,20]. Studies of the organisation of Rrp47p have revealed that the protein consists of two domains, an N-terminal Sas10/C1D-type domain spanning roughly the first 100 residues, required for binding to Rrp6p, and a C-terminal region shown to be involved in maturation of box C/D small nucleolar ribonucleoprotein (snoRNP) particles [16,21]. Finally, the extreme C-terminus of Rrp47p contains a concentrated patch of basic residues, which appears to be responsible for the majority of the RNA affinity observed *in vitro*. Interestingly, the N-terminal Sas10/C1D domain of Rrp47p is sufficient to complement nearly all of the phenotypes associated with deletion of Rrp47p in yeast [21].

In this paper, we map the interaction between yeast Rrp47p and the Rrp6p PMC2NT domain and show that complex formation leads to structural rearrangements in both proteins. Using small-angle X-ray scattering (SAXS), we determine envelopes of isolated Rrp6p as well as the Rrp6p–Rrp47p complex. Finally, we present functional evidence that Rrp47p finely modulates the activity of Rrp6p on both single-stranded and structured RNA substrates as well as affects degradation through double-stranded regions.

2. Materials and methods

2.1. Protein expression and purification

S. cerevisiae rrp47/lrp1 and *rrp6* were amplified from yeast genomic DNA and inserted into pET-30 Ek/LIC to create a single construct encoding both full length Rrp47p$^{1\text{-}184}$ (residues 1–184) and Rrp6p$^{12\text{-}536}$-His$_6$. Rrp47p–Rrp6p$^{12\text{-}536,\ D238A}$ was constructed by site-directed mutagenesis. Expression was carried out in *E. coli* BL21 (DE3) RIL (Novagen) by overnight expression at 18 °C and the complex was purified by tandem Ni^{2+}-chelating agarose chromatography (Qiagen) with Tev protease cleavage. Ion exchange chromatography using Source 15Q and Source 15S (GE Healthcare) allowed purification of both the isolated Rrp6p$^{12\text{-}536}$ (monomer and dimer) and Rrp47p$^{1\text{-}184}$, and the Rrp6p$^{12\text{-}536}$–Rrp47p$^{1\text{-}184}$ complex. Finally, all samples were purified on a Superdex 200 10/300 GL size-exclusion column (GE Healthcare) in 20 mM Tris–HCl, pH 8.0, 100 mM KCl, and 5 mM BME. See Supplementary Information for further details.

2.2. Multi-angle light scattering, SRCD, and SAXS

Multi-angle light scattering data were collected on a Zetasizer μV light scattering (Malvern Instruments) or a MiniDAWN (Wyatt Technology) system connected in-line with gel filtration. MW calculation was achieved using OmniSEC 4.7.0 (Malvern Instruments) or ASTRA (Wyatt Technology) using dn/dc = 0.187 in all cases. Synchrotron radiation circular dichroism (SRCD) spectra were collected at beam line CD1 at the ASTRID storage ring (ISA, Aarhus University, Denmark). Samples were measured in triplicate close to 1 mg/ml in 50 mM HPO_4^{2-}, pH 7.5, averaged, baseline subtracted using a buffer spectrum, and mildly smoothed using the CDtool software [22]. Synchrotron radiation SAXS data were collected at the X33 at DORIS/DESY (Hamburg, Germany) and I911-4 at MAX-Lab (Lund, Sweden) in 20 mM Tris–HCl, pH 7.5, 100 mM KCl, and 5 mM BME at 10 °C. Data were processed using ATSAS [23], *ab initio* modelling was performed using DAMMIF [24], and the most probable model was identified in DAMAVER [25]. Docking of the crystal structure was done using the SITUS package [26] and presented using Chimera [27].

2.3. In vitro RNA degradation assays and EMSA

In vitro reactions contained 10 nM 5′ carboxy-fluorescein (FAM) labelled RNA substrate (Invitrogen/Dharmacon) and 30 nM Rrp6p monomer or Rrp6p–Rrp47p complex in 12.5 mM Tris–HCl, pH 8.0, 60 mM KCl, 1.2 mM $MgCl_2$, 2.5 mM BME, and 150 nM BSA. After incubation at 30 °C, reactions were quenched with loading dye, resolved on denaturing 18% polyacrylamide gels in 1× TBE, and visualised using a Typhoon Trio Imager (GE Healthcare). Reactions for EMSA contained 10 nM synthetic 5′ FAM-labelled RNA oligo in 17.5 mM Tris–HCl, pH 8.0, 50 mM KCl, 10% glycerol, 1 mM $MgCl_2$, and 2.1 mM BME, and varying concentrations of Rrp6p$^{12\text{-}536,\ D238A}$ or its complex with Rrp47p$^{1\text{-}184}$. After incubation at room temperature for 30 min, reactions were mixed with loading dye and separated on native 8% polyacrylamide gels in 1× Tris–glycine buffer. Bands were integrated using TotalLab Quant. See Supplementary Methods for RNA sequences.

3. Results and discussion

3.1. Rrp6p–Rrp47p complex formation is associated with structural changes

S. cerevisiae Rrp6p$^{12\text{-}536}$ (residues 12–536 of 733) and Rrp47p (full length, residues 1–184) were co-expressed in *E. coli* BL21 (DE3) RIL and purified using a cleavable, C-terminal His-tag on Rrp6p (see Supplementary Methods for details and Fig. S1A). The purification also yielded pure samples of the isolated proteins (Fig. 1A and B). Consistent with previous studies, we find that the level of staining of the two proteins in pure samples of the complex suggests formation of a stoichiometric 1:1 complex between Rrp6p and Rrp47p with a theoretical molar mass of 83.2 kDa (Fig. 1A) [11,15]. For molecular mass determination, we analysed the samples by size exclusion chromatography coupled to a multi-angle static light scattering (SEC/MALS) (Fig. 1C and Table 1). The Rrp6p–Rrp47p complex elutes as a monodisperse peak with a MALS MW of 84 kDa, which is significantly smaller than the apparent MW estimated from the elution volume (~130 kDa) suggesting that the complex has a non-globular shape. Isolated Rrp47p elutes as an oligomeric species with a MALS molecular weight of app. 93 kDa, corresponding to a 4–6 mer as previously described [15,17]. Isolated Rrp6p can be separated into two distinct forms, a monomer and a dimer, which elute at two different volumes (Fig. 1C and Table 1). N-terminal sequencing reveals that the Rrp6p dimer is intact while the monomer has been cleaved near the end of the PMC2NT domain giving rise to a 85–536 fragment (Fig. 1B). This suggests that the Rrp6p PMC2NT domain is not stable in isolation, much like Rrp47p, and that interaction is required for the stability of both proteins. This is consistent with observations *in vivo* that cellular levels of Rrp47p drop when Rrp6p is depleted [17].

Finally, the secondary structure of both the isolated components and the complex was measured using synchrotron radiation circular dichroism (SRCD, Fig. 1D) [28]. Isolated Rrp6p and Rrp47p display a high α-helical content (33–35%) and lower amount of β-sheet (16–19%) consistent with crystal structure of Rrp6p [13] and predictions for Rrp47p [17]. The Rrp6p–Rrp47p complex displays a significantly higher α-helical content (42%) than either of the two constituent proteins indicating that structural differences occur upon complex formation. These values are conservative as

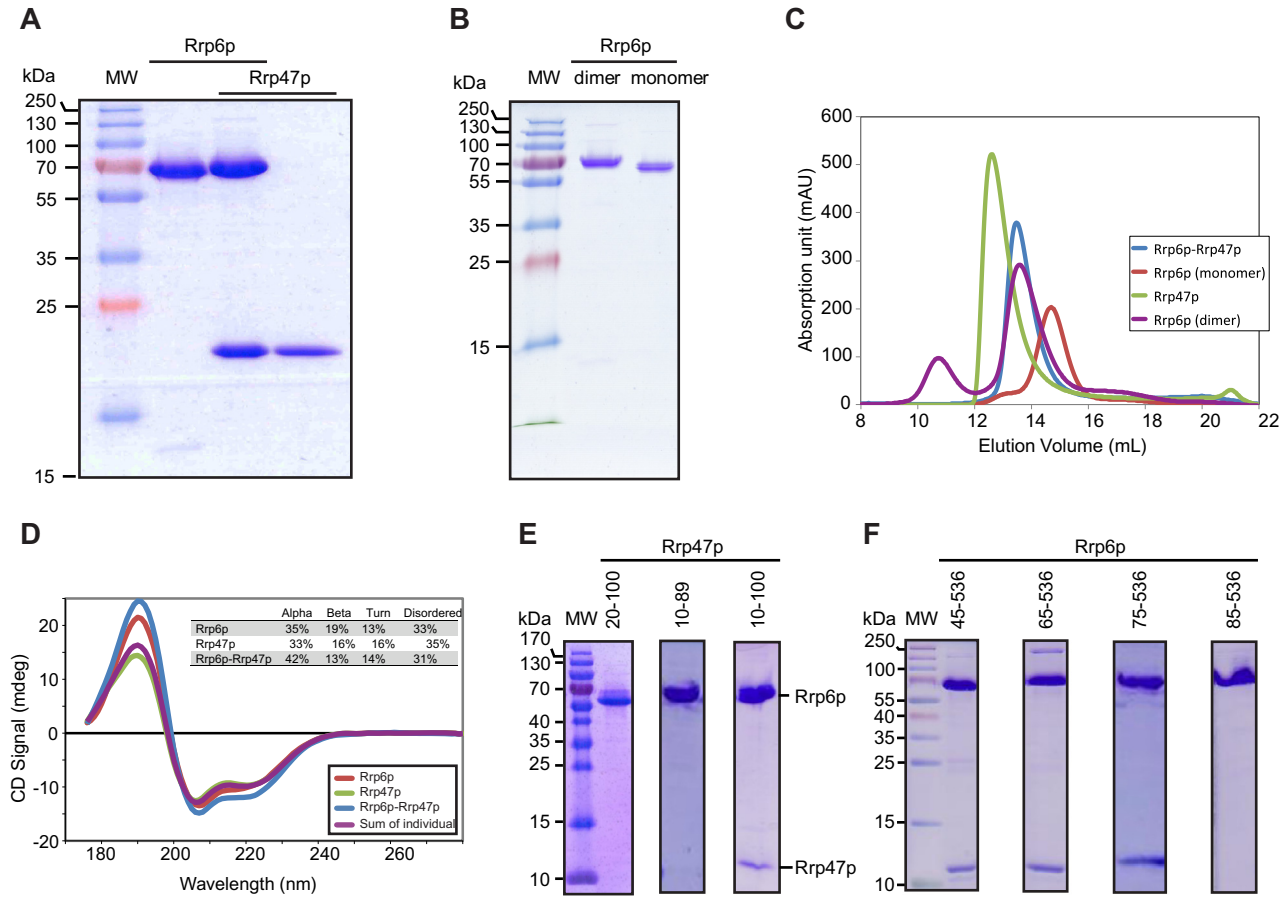

Fig. 1. Characterisation of the Rrp6p-Rrp47p complex. (A) Coomassie-stained SDS–PAGE gel showing purified samples of Rrp6p$^{12\text{-}536}$ (dimeric form), Rrp47p, and the Rrp6p$^{12\text{-}536}$–Rrp47p$^{1\text{-}184}$ complex. (B) As (A) showing purified samples of the Rrp6p dimer and monomer (85–536) forms. (C) UV-absorption (A_{280}) profiles showing elution of Rrp6p (monomer, red and dimer, purple), Rrp47p$^{1\text{-}184}$ (green), and the Rrp6p$^{12\text{-}536}$–Rrp47p (blue) complex during SEC. (D) SR-CD spectra collected from isolated Rrp6p (red), Rrp47p (green), and the Rrp6p–Rrp47p complex (blue). The sum of the measurements for the individual proteins (purple) is shown for comparison. The inset table shows calculated secondary structure content. (E) As (A) showing pull-downs of Rrp6p$^{12\text{-}536}$-His co-expressed with the Rrp47p Sas10/C1D domain on either the 20–100, 10–89, or 10–100 forms. (F) As (A) showing pull-downs of several forms of Rrp6p-His co-expressed with the Rrp47p$^{1\text{-}100}$ Sas10/C1D domain. (For interpretation of the references to colour in this figure legend, the reader is referred to the web version of this article.)

Table 1
Measured molecular masses and stoichiometries. Molecular weight (MW) estimates.

	MW^{SEC} (kDa)	MW^{MALS} (kDa)	MW^{SAXS} (kDa)	Theoretical MW (kDa)	Oligomer
Rrp6p	82	67	56	55	Monomer
	116	94	114	124.4	Dimer
Rrp47p	N.O.	N.O.	N.O.	21	Monomer
	116	93 ± 16	N.D.	84–126	4–6 mer
Rrp6p–Rrp47p	130	84	97	83.2	1:1 complex

the isolated proteins are already partially stabilised by oligomerisation and are consistent with the requirement of each protein for their binding partner for stability *in vivo* [20,29].

3.2. The Rrp47p Sas10/C1D domain interacts with a conserved N-terminal region of Rrp6p

The N-terminal Sas10/C1D domain of Rrp47p (residues 1–100) is known to interact directly with the PMC2NT domain of Rrp6p (Fig. S1A) [17,21]. To analyse the interaction in more detail, we constructed several truncated versions of both proteins and asked using His pull-downs of Rrp6p whether the complex was still intact (Fig. 1E and F). Pull-down of Rrp6p$^{12\text{-}536}$ co-expressed with Rrp47p$^{10\text{-}100}$ confirmed that the Sas10/C1D domain alone is sufficient for stable complex formation (Fig. 1E). Further truncation of Rrp47p, however, caused the complex to break, showing that the intact Sas10/C1D domain is required for complex formation (Fig. 1E, lanes 20–100 and 10–89). The N-terminus of Rrp47p is not highly conserved but is predicted to be helical and therefore likely disturbed by the truncations (Fig. S1B and S2). At the end of the Sas10/C1D domain, conservation stretches up to residue 93, consistent with the observation that Rrp47p$^{10\text{-}89}$ is not able to bind Rrp6p. To map the interaction on the Rrp6p side, truncations were made to produce variants of Rrp6p starting at residue 45, 65, 75, and 85 co-expressed with Rrp47p$^{1\text{-}100}$ (Fig. 1F). Of these, Rrp47p bound to all except Rrp6p$^{85\text{-}536}$ suggesting that the interaction with Rrp47p takes place via the 75–129 region of Rrp6p, which is more conserved than the very N-terminus (Fig. S1B and S2). In summary, we conclude that the minimal interaction regions of Rrp6p and Rrp47p involve the PMC2NT domain of Rrp6p starting

at residue 75 and the core Sas10/C1D domain of Rrp47p (residues 1–100).

3.3. Rrp47p binds on top of the Rrp6p exonuclease core domain

We next analysed Rrp6p on both dimer and monomer forms as well as the Rrp6p$^{12-536}$–Rrp47p$^{1-184}$ (full-length Rrp47p), Rrp6p$^{12-536}$–Rrp47p$^{1-100}$ (Sas10/C1D domain), and Rrp6p$^{75-536}$–Rrp47p$^{1-100}$ (minimal interaction region) complexes by synchrotron small-angle X-ray scattering (SAXS) and used the data for *ab initio* modelling using the dummy-atom approach (Fig. S3) [24]. The SAXS envelope obtained for the Rrp6p monomer is compact and fits well to the crystal structure of yeast Rrp6p (PDB 2HBJ, Fig. 2A) [13]. Extra density on the side and on top of the exonuclease core accounts for the part of the PMC2NT domain not present in the crystal structure. Likewise, modelling of the Rrp6p dimer (residues 12–536) resulted in a symmetric, flat shape that allows docking of two copies of Rrp6p including PMC2NT domains (Fig. S4A) [13]. The envelope calculated for the Rrp6p$^{12-536}$–Rrp47p$^{1-184}$ complex is also elongated and has approximately the same dimensions (D_{max} = 136 Å) as the Rrp6p dimer (D_{max} = 141 Å, Fig. 2B, S4B and Table T1), consistent with the co-elution of the two samples during gel filtration (Fig. 1C). However, the complex envelope is not symmetrical and consists of one extended (bottom) and one more globular (top) end (Fig. 2B). The exonuclease domain of Rrp6p fits accurately into the envelope with the HRDC domain at the bottom and with density next to and on top of the exonuclease core to account for the PMC2NT domain and Rrp47p. The SAXS envelopes calculated for Rrp6p$^{12-536}$–Rrp47p$^{1-100}$ and Rrp6p$^{75-536}$–Rrp47p$^{1-100}$ have very similar shapes to the more intact complex and the extension assigned to the HRDC domain of Rrp6p is consistently present in all models (Figs. 2C and D and S4B). Furthermore, the density assigned to the PMC2NT domain/Rrp47p gets progressively smaller as the complex is truncated, which is also reflected in progressively smaller Porod volumes (165, 147, and 130 nm^3, respectively), while D_{max} remains almost constant (Fig. S4B and Table T1). In conclusion, we have shown that the Rrp6p–Rrp47p complex has an elongated shape consistent with gel filtration chromatography, significantly larger than monomeric Rrp6p but with similar dimensions to dimeric Rrp6p. Docking of the crystal structure of Rrp6p suggests that Rrp47p binds on top of the exonuclease domain, in contact with the PMC2NT and opposite of the HRDC domain. Although this position does not preclude a direct interaction of Rrp47p with RNA, Rrp47p is relatively distant from the active site on Rrp6p in this model. As Rrp6p is known to interact with the exosome via its C-terminus, this model further suggests that Rrp47p binds away from the exosome core (Fig. 4) [10]. RNA substrates directed to the exosome can then either enter Rrp6p directly or pass through the core for degradation by Rrp44p.

3.4. Rrp47p subtly affects the activity of Rrp6p on both single-stranded and structured RNA

The activities of yeast and human Rrp6p have previously been characterised *in vitro* showing that the enzymes are able to degrade a range of RNA substrates in a 3′–5′ directed fashion with a subtle preference for poly-A stretches, reflecting the role of Rrp6p

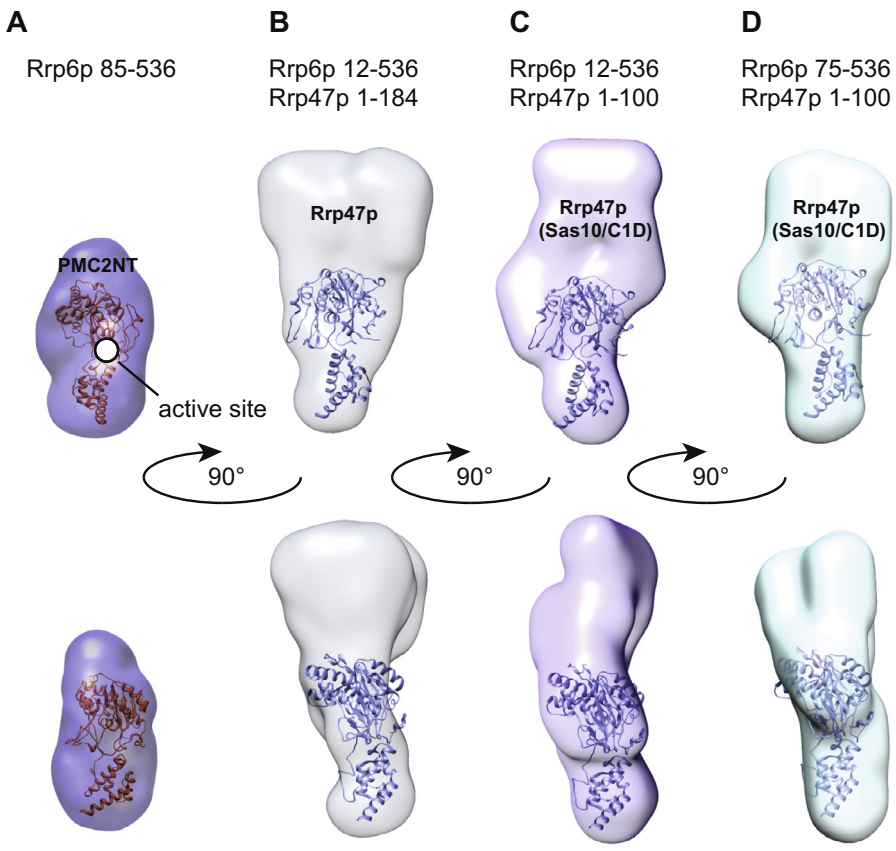

Fig. 2. Rrp47p binds on top of the Rrp6p exonuclease core domain. (A) SAXS *ab initio* envelope of Rrp6p (monomer, 85–536) based on dummy-atom modelling in two orthogonal views showing docking of the crystal structure of Rrp6p (129–536, PDB 2HBJ) [13]. "PMC2NT" is the position of the part of Rrp6p missing from the crystal structure. (B) As (A) showing the Rrp6p$^{12-536}$–Rrp47p$^{1-184}$ complex, where "Rrp47p" indicates the position of the combined Rrp47p–PMC2NT interaction domain. (C) As (A) showing the Rrp6p$^{12-536}$–Rrp47p$^{1-100}$ Sas10/C1D complex. (D) As (A) showing the Rrp6p$^{75-536}$–Rrp47p$^{1-100}$ minimal interaction region complex. All figures were made using PyMOL and UCSF Chimera [27].

in scavenging nuclear poly-adenylated transcripts *in vivo* [3,7,12]. Recent functional studies of Trypanosoma RRP6 bound to the Rrp47p orthologue, EAP3, showed that the co-factor slows down the nuclease marginally, but doesn't affect the specificity or ability of the enzyme to degrade double-stranded RNA [11]. To investigate activity of yeast Rrp6p–Rrp47p, we carried out a series of *in vitro* RNA degradation assays with defined, 5′ fluorescently labelled RNA substrates. All comparisons were made between co-purified Rrp6p$^{12\text{-}536}$–Rrp47p$^{1\text{-}184}$ complex and isolated Rrp6p monomer originating from the same purification and at conditions where

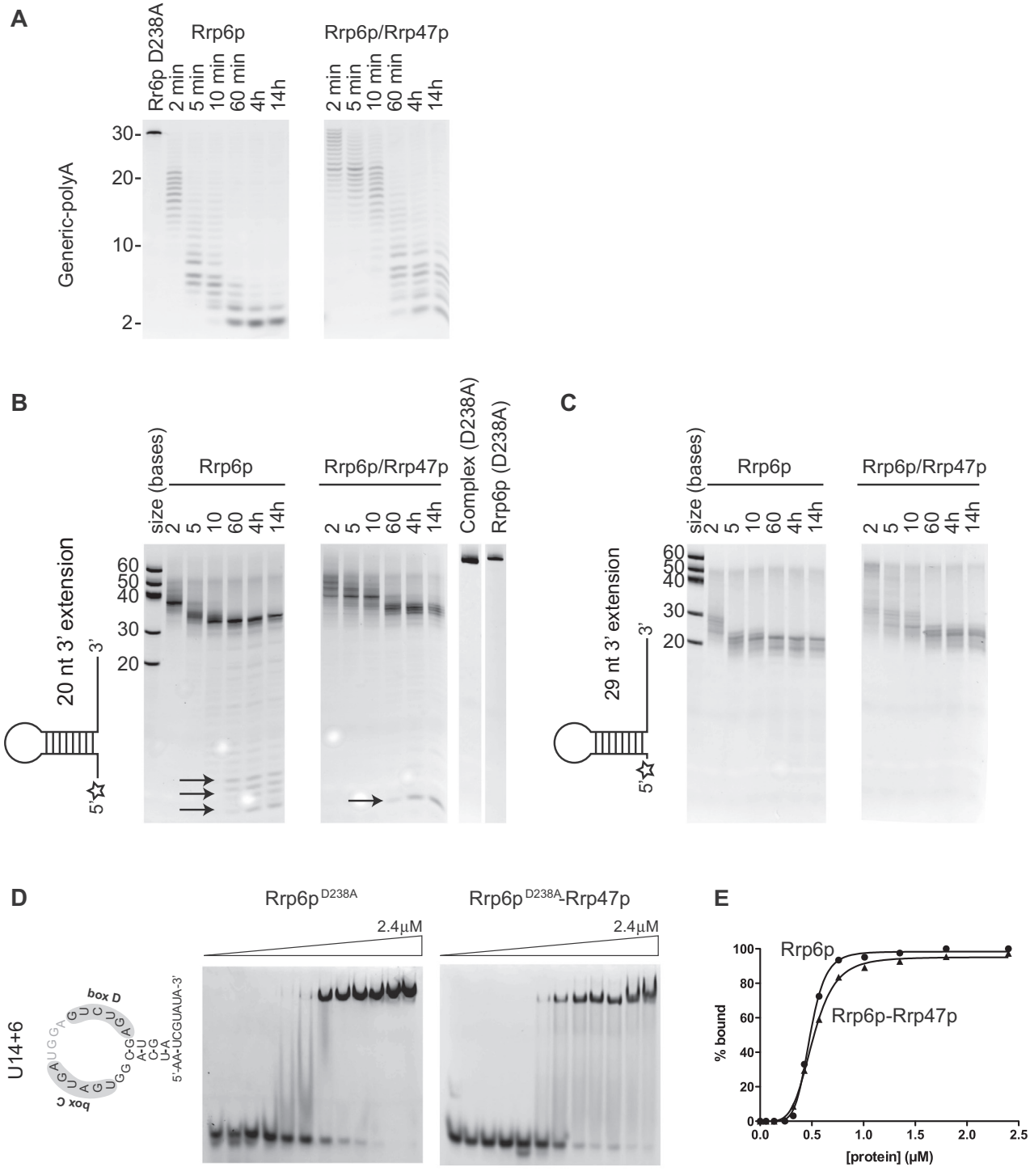

Fig. 3. Rrp47p modulates Rrp6p activity but not RNA affinity. (A) *In vitro* degradation experiments using a defined single-stranded, 5′-labelled RNA substrates with a poly-adenosine (A) 3′-end sequence (Generic-polyA). Experiments were carried out with isolated Rrp6p (monomer) or the Rrp6p$^{12\text{-}536}$–Rrp47$^{1\text{-}184}$ complex and the resulting 5′ RNA fragments separated by denaturing PAGE and visualised by scanning fluorometry. For the lane marked "Rrp6p D238A", the inactive D238A mutant of Rrp6p was used as control for contaminating *E. coli* nucleases. (B) As (A) showing reactions with structured and 5′-labelled RNA substrate with 5′ extension as indicated. The star marks the position of the fluorescent label and the arrows indicate where degradation has proceeded through RNA secondary structure. Both the Rrp6p–Rrp47p complex and isolated Rrp6p purified as inactive D238A mutants are included as controls for contamination. (C) As (B) but using a substrate with no 5′ extension. (D) EMSA using a fixed amount (10 nM) of U14 pre-snoRNA substrate and increasing concentrations (0–2.4 μM) of either Rrp6p$^{12\text{-}536,\ D238A}$ or the Rrp6p$^{12\text{-}536,\ D238A}$–Rrp47p$^{1\text{-}184}$ complex. (E) Binding curves obtained for Rrp6p (●) and the Rrp6p–Rrp47p complex (▲) calculated as % bound RNA based on integration of the gel bands.

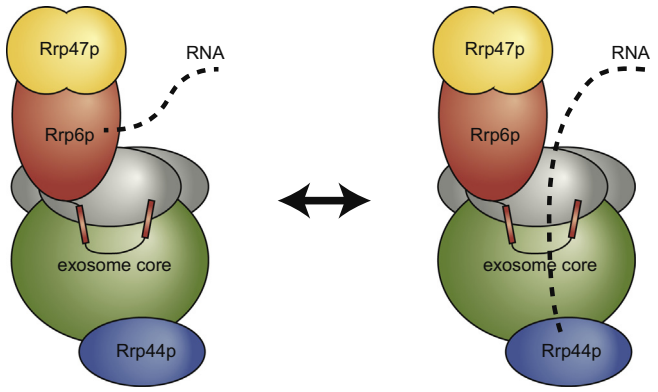

Fig. 4. A model for the interaction of Rrp6p–Rrp47 with the exosome core. RNA degradation by the yeast nuclear exosome may proceed either directly by the Rrp6p–Rrp47p complex or by Rrp44p following threading through the exosome core barrel.

the enzyme concentration (30 nM) exceeded that of RNA (10 nM). First, we compared the activities towards a 30-mer Generic-polyA RNA substrate consisting of 20 nt of constant, generic sequence followed by 10 nt oligo-A. This substrate is rapidly degraded by Rrp6p down to about 2 nucleotides (Fig. 3A). Notably, the oligo-A tail (residues 20–30) appears to be degraded much faster than the remaining body of the RNA. Like for Trypanosoma RRP6, degradation is about 5–10-fold slower in the presence of Rrp47p as seen from comparison of the 10 min and 2 min time points [11]. Similarly to isolated Rrp6p, the complex degrades the 10 nt oligo-A tail much more efficiently. In contrast to Trypanosoma RRP6, however, we find that yeast Rrp6p is generally not able to degrade stable, RNA secondary structure. For human RRP6 it was shown that the presence of a 5′ extended single-stranded region in front of a stable structured hairpin somehow allows Rrp6p to proceed through the double-stranded region [12]. We therefore asked whether the presence of Rrp47p would affect the ability of Rrp6p to degrade stable RNA secondary structure by analysing degradation of substrates containing a strong hairpin followed by an extended 3′ single-stranded region and with (Fig. 3B) or without (Fig. 3C) a 5′ extension. Consistent with the observations for human RRP6, we observe that yeast Rrp6p is able to proceed through the RNA hairpin structure in the presence of a 5′ single-stranded extension (Fig. 3B, marked with arrows) but not when this element is missing (Fig. 3C). In the presence of Rrp47p, the activity of Rrp6p is reduced but appears to eventually reach the same end-point. However, we note that degradation by the complex through the hairpin proceeds with fewer intermediate bands than for isolated Rrp6p (arrows), suggesting that although Rrp47p appears to reduce overall rate of the Rrp6p reaction, degradation through the hairpin is not affected to the same extent. This suggests that the mechanism by which Rrp6p degrades secondary structure is not affected by binding of Rrp47p to the same extent as degradation of single-stranded RNA.

3.5. Rrp47p does not affect the affinity of Rrp6p towards structured RNA

To investigate whether Rrp47p contributes to RNA affinity in the Rrp6p–Rrp47p complex, we analysed the binding of monomeric Rrp6p (85–536) and the Rrp6p$^{12\text{-}536}$–Rrp47p$^{1\text{-}184}$ complex to defined RNAs including both single-stranded and structured regions by electrophoretic mobility shift assays (EMSA). Our hypothesis was that if both proteins contribute to RNA binding, a significant increase in the measured affinity should distinguish the complex from the isolated nuclease. The RNA substrates used were a range of 32–35 nt mimics of yeast U14 pre-snoRNA, which is naturally processed by Rrp6p in a Rrp47p-dependent manner [18]. Of these, the substrate U14 + 6 contains both single-stranded and structured elements, including the conserved terminal stem and the box C/D elements characteristic of these RNAs in addition to a 3–6 residue extension mimicking a 3′ unprocessed pre-snoRNA (Fig. 3D). In both cases, dissociation constants were measured using the Rrp6p^{D238A} active site to prevent RNA degradation during the experiment. For all tested RNAs (some data not shown) isolated Rrp6p and the Rrp6p$^{12\text{-}536}$–Rrp47p$^{1\text{-}184}$ complex showed very similar dissociation constants (K_D) in the low micro-molar range, suggesting that Rrp47p affects the activity of Rrp6p in a way not related to binding affinity (Fig. 3E). Taken together with the observed changes in activity, our data collectively support a model in which Rrp47p affects Rrp6p activity allosterically, most likely without direct interaction with the substrate. To elucidate the details of the mechanistic interplay between these important cofactors of the nuclear RNA exosome, a high-resolution structural analysis of the Rrp6p–Rrp47p complex, and if possible, their interaction with the exosome core will be required.

Conflict of interest

The authors declare no conflicts of interest.

Acknowledgments

We thank the beam line staff at X33 at DESY and I911-4 at MAX-Lab for help with the SAXS experiments. The Danish Council for Independent Research (FNU) [09-072378] and the Danish National Research Foundation Centre for mRNP Biogenesis and Metabolism funded this project. The ERC Advanced Research Program, Biomemos, supported T.B.

Appendix A. Supplementary data

Supplementary data associated with this article can be found, in the online version, at http://dx.doi.org/10.1016/j.bbrc.2014.06.032.

References

[1] S. Lykke-Andersen, D.E. Brodersen, T.H. Jensen, Origins and activities of the eukaryotic exosome, J. Cell Sci. 122 (2009) 1487–1494.
[2] P. Mitchell, E. Petfalski, A. Shevchenko, M. Mann, D. Tollervey, The exosome: a conserved eukaryotic RNA processing complex containing multiple 3′ → 5′ exoribonucleases, Cell 91 (1997) 457–466.
[3] Q. Liu, J.C. Greimann, C.D. Lima, Reconstitution, activities, and structure of the eukaryotic RNA exosome, Cell 127 (2006) 1223–1237.
[4] E. Lorentzen, J. Basquin, E. Conti, Structural organization of the RNA-degrading exosome, Curr. Opin. Struct. Biol. 18 (2008) 709–713.
[5] A. Dziembowski, E. Lorentzen, E. Conti, B. Seraphin, A single subunit, Dis3, is essentially responsible for yeast exosome core activity, Nat. Struct. Mol. Biol. 14 (2007) 15–22.
[6] A. Lebreton, R. Tomecki, A. Dziembowski, B. Seraphin, Endonucleolytic RNA cleavage by a eukaryotic exosome, Nature 456 (2008) 993–996.
[7] J. Assenholt, J. Mouaikel, K.R. Andersen, D.E. Brodersen, D. Libri, T.H. Jensen, Exonucleolysis is required for nuclear mRNA quality control in yeast THO mutants, RNA 14 (2008) 2305–2313.
[8] M.W. Briggs, K.T. Burkard, J.S. Butler, Rrp6p, the yeast homologue of the human PM-Scl 100-kDa autoantigen, is essential for efficient 5.8 S rRNA 3′ end formation, J. Biol. Chem. 273 (1998) 13255–13263.
[9] S. Phillips, J.S. Butler, Contribution of domain structure to the RNA 3′ end processing and degradation functions of the nuclear exosome subunit Rrp6p, RNA 9 (2003) 1098–1107.
[10] D.L. Makino, M. Baumgartner, E. Conti, Crystal structure of an RNA-bound 11-subunit eukaryotic exosome complex, Nature 495 (2013) 70–75.
[11] R.L. Barbosa, P. Legrand, F. Wien, B. Pineau, A. Thompson, B.G. Guimaraes, RRP6 from *Trypanosoma brucei*: crystal structure of the catalytic domain, association with EAP3 and activity towards structured and non-structured RNA substrates, PLoS One 9 (2014) e89138.
[12] K. Januszyk, Q. Liu, C.D. Lima, Activities of human RRP6 and structure of the human RRP6 catalytic domain, RNA 17 (2011) 1566–1577.
[13] S.F. Midtgaard, J. Assenholt, A.T. Jonstrup, L.B. Van, T.H. Jensen, D.E. Brodersen, Structure of the nuclear exosome component Rrp6p reveals an interplay

between the active site and the HRDC domain, Proc. Natl. Acad. Sci. U.S.A. 103 (2006) 11898–11903.
[14] Y. Zuo, Y. Wang, A. Malhotra, Crystal structure of *Escherichia coli* RNase D, an exoribonuclease involved in structured RNA processing, Structure 13 (2005) 973–984.
[15] M. Feigenbutz, R. Jones, T.M. Besong, S.E. Harding, P. Mitchell, Assembly of the yeast exoribonuclease Rrp6 with its associated cofactor Rrp47 occurs in the nucleus and is critical for the controlled expression of Rrp47, J. Biol. Chem. 288 (2013) 15959–15970.
[16] P. Mitchell, Rrp47 and the function of the Sas10/C1D domain, Biochem. Soc. Trans. 38 (2010) 1088–1092.
[17] J.A. Stead, J.L. Costello, M.J. Livingstone, P. Mitchell, The PMC2NT domain of the catalytic exosome subunit Rrp6p provides the interface for binding with its cofactor Rrp47p, a nucleic acid-binding protein, Nucleic Acids Res. 35 (2007) 5556–5567.
[18] P. Mitchell, E. Petfalski, R. Houalla, A. Podtelejnikov, M. Mann, D. Tollervey, Rrp47p is an exosome-associated protein required for the 3′ processing of stable RNAs, Mol. Cell. Biol. 23 (2003) 6982–6992.
[19] A. van Hoof, P. Lennertz, R. Parker, Yeast exosome mutants accumulate 3′-extended polyadenylated forms of U4 small nuclear RNA and small nucleolar RNAs, Mol. Cell. Biol. 20 (2000) 441–452.
[20] M. Feigenbutz, W. Garland, M. Turner, P. Mitchell, The exosome cofactor Rrp47 is critical for the stability and normal expression of its associated exoribonuclease Rrp6 in *Saccharomyces cerevisiae*, PLoS One 8 (2013) e80752.
[21] J.L. Costello, J.A. Stead, M. Feigenbutz, R.M. Jones, P. Mitchell, The C-terminal region of the exosome-associated protein Rrp47 is specifically required for box C/D small nucleolar RNA 3′-maturation, J. Biol. Chem. 286 (2011) 4535–4543.
[22] J.G. Lees, B.R. Smith, F. Wien, A.J. Miles, B.A. Wallace, CDtool-an integrated software package for circular dichroism spectroscopic data processing, analysis, and archiving, Anal. Biochem. 332 (2004) 285–289.
[23] P.V. Konarev, M.V. Petoukhov, V.V. Volkov, D.I. Svergun, ATSAS 2.1, a program package for small-angle scattering data analysis, J. Appl. Cryst. 39 (2006) 277–286.
[24] D. Franke, D.I. Svergun, DAMMIF, a program for rapid ab-initio shape determination in small-angle scattering, J. Appl. Cryst. 42 (2009) 342–346.
[25] V.V. Volkov, D.I. Svergun, Uniqueness of ab initio shape determination in small-angle scattering, J. Appl. Cryst. 36 (2003) 860–864.
[26] W. Wriggers, Using situs for the integration of multi-resolution structures, Biophys. Rev. 2 (2010) 21–27.
[27] E.F. Pettersen, T.D. Goddard, C.C. Huang, G.S. Couch, D.M. Greenblatt, E.C. Meng, T.E. Ferrin, UCSF chimera – a visualization system for exploratory research and analysis, J. Comp. Chem. 25 (2004) 1605–1612.
[28] L. Whitmore, B.A. Wallace, Protein secondary structure analyses from circular dichroism spectroscopy: methods and reference databases, Biopolymers 89 (2008) 392–400.
[29] I. Stuparevic, C. Mosrin-Huaman, N. Hervouet-Coste, M. Remenaric, A.R. Rahmouni, Cotranscriptional recruitment of RNA exosome cofactors Rrp47p and Mpp6p and two distinct Trf-Air-Mtr4 polyadenylation (TRAMP) complexes assists the exonuclease Rrp6p in the targeting and degradation of an aberrant messenger ribonucleoprotein particle (mRNP) in yeast, J. Biol. Chem. 288 (2013) 31816–31829.